Spike Response Properties of an AER EAR

Vincent Chan[#], André van Schaik[#] and Shih-Chii Liu[*]

[#]School of Electrical and Information Engineering
University of Sydney
Sydney, NSW 2006, Australia

[*]Institute of Neuroinformatics
ETH/University of Zürich,
Zürich, CH-8057, Switzerland

ABSTRACT

We present measured frequency-gain functions and the spike rate outputs of the different sections in a spiking silicon cochlea chip. The chip consists of a matched pair of silicon cochleae with an address event interface for the output. Each section of the cochlea is modelled by a second-order low-pass filter followed by a simplified Inner Hair Cell circuit and a Spiking Neuron circuit. When the neuron spikes, an Address Event is generated on the asynchronous data bus. These spike outputs are analogous to the spikes on an auditory nerve, connecting the cochlea with the brain.

1. INTRODUCTION

For multi-chip neuromorphic systems, the Address Event Representation (AER) interface has become the standard interface protocol. The AER approach allows us to model biological systems using discrete level (spikes) and continuous time events to convey information, similar to the pulse code neural communication and processing systems found in living organisms. This representation is ideal for communicating sparse events from many sources using a narrow channel [1, 2].

AER allows multiple devices to share a common data bus by using a hand-shaking protocol that arbitrates between transmitters to determine which transmitter can access the bus. The next transmission is not permitted unless an acknowledgement is returned from the receiver. This method allows multiple transmitters to communicate with multiple receivers in a pseudo-parallel fashion. Since the events are generated asynchronously, random ordering of transmissions occurs, producing Poisson distributed event streams which, statistically, preserve the timing between events [3]. Furthermore, the event stream models the timing relationships of biological synaptic transmission very well.

In addition to allowing multiple sensors to communicate to multiple processors using a common bus, the AER protocol can be used to perform computation through the manipulation of the statistics and routing of events from the input stream. For example, spatial filtering on a receiver chip can be realized if each pixel in the transmitter array transmits a projection field to the receiver chip.

To date, the AER protocol has almost exclusively been used in vision chips (e.g. [3,4,5,6,7,8,9,10]) and some neural processors (e.g. [11,12,13,14,15]). The only silicon cochleae with an Address Event type representation that the authors are aware of are [16], [17], and [18], but these implementations use a very small silicon cochlea (9, 15, and 8 sections, respectively), and a non-standard implementation of the AER protocol. Furthermore,

in [17], only the zero-crossings of the output signal of each cochlear section were preserved. Last year we presented our AER EAR containing two silicon cochleae with AER output and some preliminary sound localization results [19]. Here we present measurements to determine the frequency-gain functions that indicate the matching of the silicon cochleae and the AER spike rate of each cochlea stage as a function of frequency.
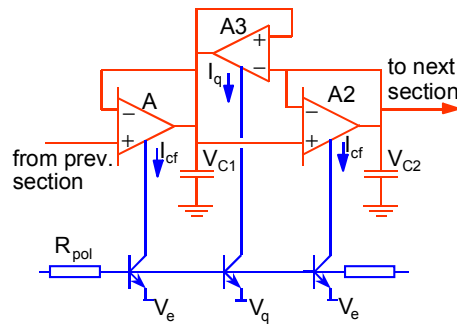

Figure 1. The second order section used in the cochleae.

2. THE SILICON COCHLEA

The silicon cochlea used is identical to the one we have presented in [20]. It is a modern version of the one presented in [21], which had already proven its use in other neuromorphic sound processing systems [22, 23]. The basic building block for the filters in this cochlear model is a second order low-pass filter section show in Figure 1. It is built with transconductance amplifiers operating in weak inversion. For input voltages smaller than about 60 mV$_{pp}$, the amplifier can be approximated as a linear transconductance:

$$I_{out} = g_m(V_{in+} - V_{in-}) \tag{1}$$

with transconductance g_m given by:

$$g_m = \frac{I_0}{2nU_T} \tag{2}$$

where I_0 is the bias current, n is the slope factor, and the thermal voltage $U_T = kT/q = 25.6$ mV at room temperature. If all three amplifiers in the circuit are identical, this second-order section may be stable for small signals, but will exhibit large signal instability due to slew-rate limitations [24]. This can be solved by using a transconductance amplifier with a wider linear input range in the forward path [24]. This also allows larger input signals to be used, up to about 140 mVpp.
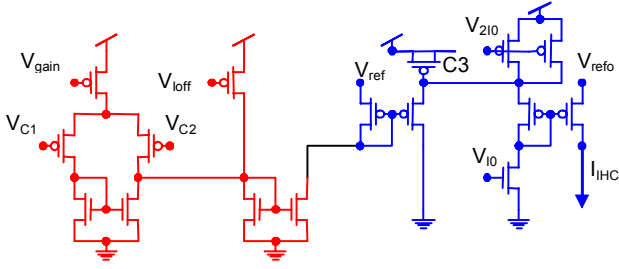
ISCAS 2006

Figure 2. The simplified Inner Hair Cell.

Figure 3. The AER spiking neuron.

Our silicon cochlea is implemented by cascading 32 of these second-order low-pass sections with exponentially decreasing cut-off frequencies. The exponential decrease is obtained by creating the bias currents of the second-order section with CMOS Compatible Lateral Bipolar Transistors, as proposed in [21]. A band-pass filtered output is obtained from each section by taking $V_{C1} - V_{C2}$ as the differential output signal.

3. INNER HAIR CELL & AER OUTPUT

In the biological cochlea the Inner Hair Cells transduce vibration in the cochlea into a neural signal. A simplified Inner Hair Cell circuit is shown in Figure 2. A transconductance amplifier transforms the differential cochlear output into a single ended current, to which a DC offset may be added using V_{Ioff}. The gain of the conversion can be set with V_{gain}. A current mirror rectifies the current signal before passing it through a first-order log-domain low-pass filter. The cut-off frequency of the low-pass filter can be controlled with V_{I0} and V_{2I0}, which generate bias currents I_0 and $2I_0$, respectively. The cut-off frequency is directly proportional to I_0 and is set around 1 kHz as in the real Inner Hair Cell. This low pass filtering models the reduction in phase-locking observed on real Auditory Nerves at frequencies greater than 1 kHz. Therefore, at input frequency above a few kHz, the output is an almost constant current and only magnitude information is preserved. The gain of the low-pass filter is exponentially proportional to $V_{ref} - V_{refo}$. In the results shown here, both voltages were equal (4.5V), resulting in a gain of 1.

The output current I_{IHC} is passed through a current mirror (not shown) which is cascaded with V_{cas}, shown in Figure 3. This point forms the boundary between the analogue front-end and the digital AER circuits. The analogue and digital circuits run on separate power supplies to reduce digital noise on the analogue signals.

When the acknowledge signal (ack) is low, I_{IHC} is integrated onto the membrane capacitor C_m of the neuron circuit, which has a leak controlled by V_{th}. The spike is generated by two inverters in series, with positive feedback through C_{fb}. When a spike is generated the request line (req) is pulled low. A high pulse in acknowledgement (ack) resets the neuron after which it will enter a refractory period with a duration controlled by $V_{refract}$. The AER protocol is arbitered as in [1]. When a neuron pulls the request line low, the arbiter will check if the data bus is free and when it is will put the neuron's address on the bus and acknowledge the neuron, which will reset it.
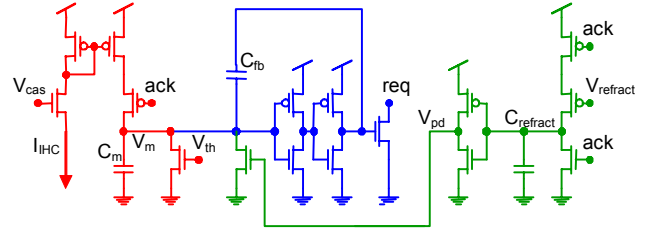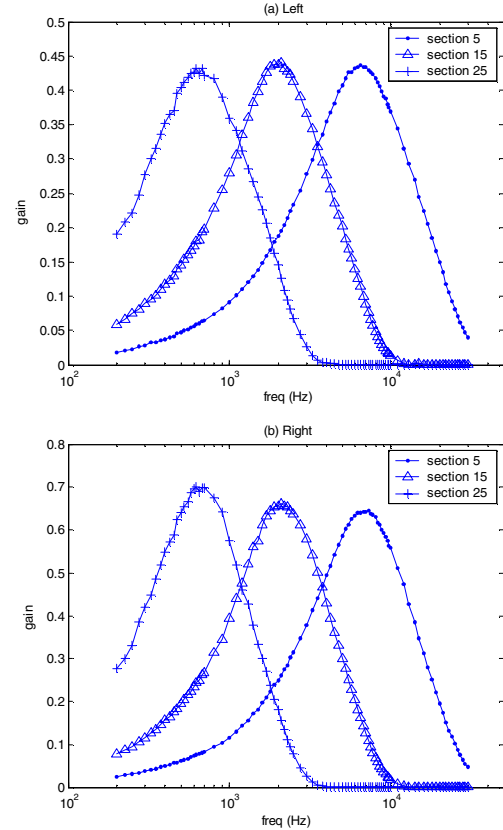

Figure 4. Measured frequency response of V_{C1}-V_{C2} at sections 5, 15 and 25 of (a) the left cochlea and (b) the right cochlea

4. MEASUREMENT RESULTS

We measure the frequency response at each filter section by measuring the differential voltage V_{C1}-V_{C2} via a scanner. The sections are numbered from 1 (highest frequency) to 32 (lowest frequency). A 150mVpp sine wave with frequency varying from 200Hz to 30kHz is applied to the input of both cochleae and the peak-to-peak amplitude of the differential output signal V_{C1}-V_{C2} is measured. The gain, expressed as the ratio between input and output peak-to-peak amplitude, is shown in Figure 4 as a function of frequency. It shows that the shape of the response is invariant of frequency when plotted on a log-frequency axis. The gains across the 32 sections are also very consistent, although there is a difference in gain between sections in the left cochlea and those in the right. On all the chips that we have measured, the right

cochlea is found to have a gain systematically 3 to 4dB higher. This is probably due to the large difference in length of wiring from the second-order section to the scanner between the two cochleae and will be corrected in future versions.

At the Inner Hair Cell (IHC), this differential signal (V_{C1}-V_{C2}) is converted to current, half-wave rectified and filtered. This current then drives an integrate-and-fire neuron, producing spikes on the AER bus. In biology, the spike rate on the auditory nerve is limited to about 100 spikes per second, but a number of nerve fibres originate from the same IHC and many IHCs code for a similar frequency range. In our case we only have 32 filters for almost two octaves of input frequency range and only one AER neuron per IHC. Therefore, to obtain enough spikes from each filter we have given the IHC circuit a high gain through lowering V_{gain} (Figure 2) and decreasing $V_{refract}$ (Figure 3), so that the maximum spike rate of the AER neuron is more than 10000 spikes per second. The firing rates of the neuron in the same channels as in Figure 4 are shown as a function of frequency in Figure 5, demonstrating the frequency selectivity of the cochleae.
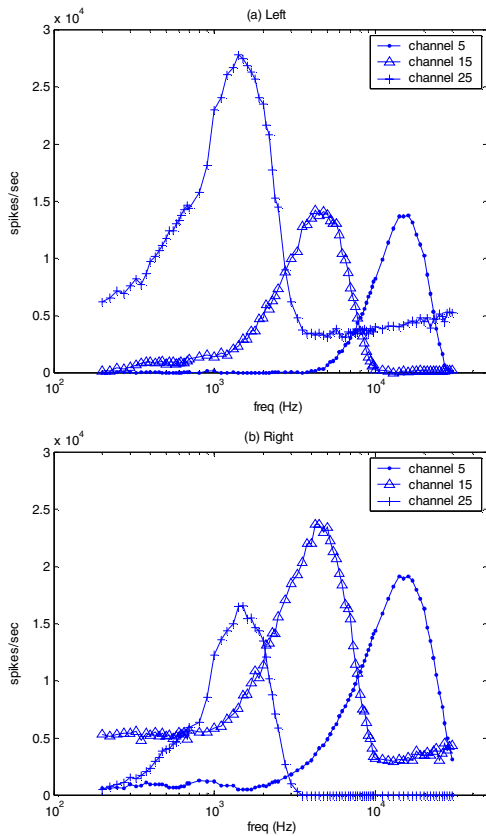

Figure 5. Spike rates of neurons in selected channels.

Comparing the spike rates in Figure 5 with the frequency responses at Figure 4, we see that they peak at different frequencies. This is a measurement artifact, due to an increase in capacitance at C1 and C2 when they are loaded during frequency response measurement, as no on-chip buffering is provided.

It can be seen that there are large variations in the spike rate offset, with some neurons spiking even when the input signal is

well outside the pass-band. In fact, these neurons will spike in the absence of any input. This is caused by a dc offset between V_{C1} and V_{C2} in the second-order section due to mismatch, producing a constant offset current I_{IHC}. There are also some variations in gain between the output of the cochleae and the spike rate of the corresponding neuron. This comes from mismatch in the Inner Hair Cell circuitry as well as in the neuron itself. Furthermore, the leakage current of the AER neurons will be sensitive to variations in threshold voltage. However, the overall frequency selectivity is preserved.
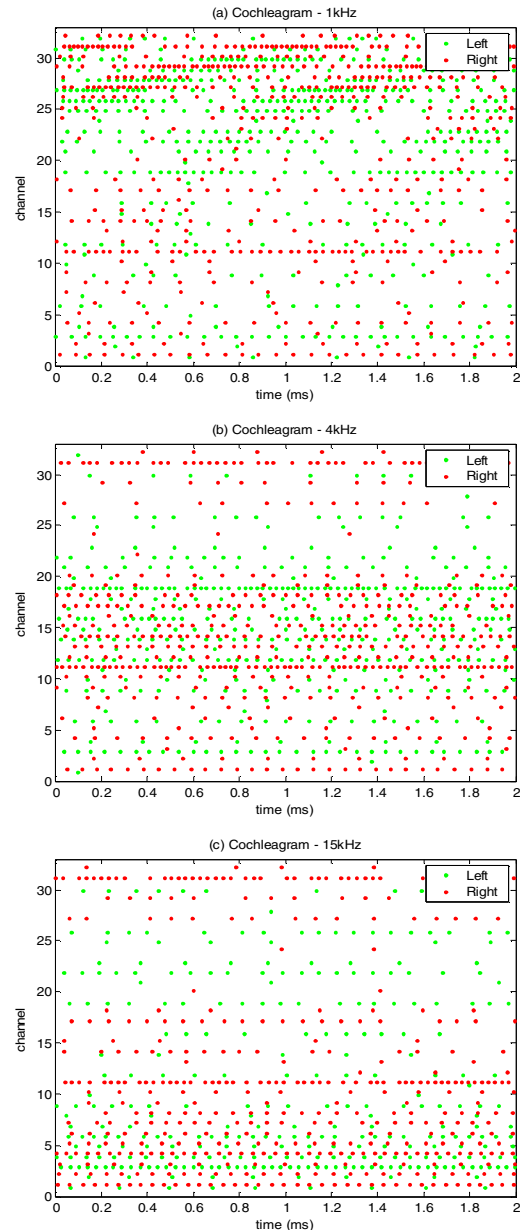

Figure 6. Cochleagrams for different sinusoidal inputs. (a) 1kHz, (b) 4kHz, and (c) 15kHz. Phase-locking can be seen for 1kHz, but disappear at 4kHz due to IHC low-pass filtering

In Figure 6 we show the spikes as a function of time in each of the cochlear channels for three different input frequencies. Again we see that some neurons fire significantly more than others. In Figure 6a, we can see that for a 1kHz input signal, phase locking of the spikes to the input signal is preserved, as the spike density varies with a 1kHz rate. At 4kHz and 15kHz, this phase locking is absent. As explained in the previous section, this models the phase locking at biological auditory nerves that is present for low frequency signal.

5. CONCLUSION

In this paper we have presented the gain-frequency measurements of our AER cochlea. The cochlea can operate over a wide range of audio frequency and its response is very consistent. Despite the variation in firing rate due to mismatches and offsets, it is capable of extracting frequency information from an input signal. A future version of this AER cochlea will focus on reducing these variations and increasing the frequency selectivity of each channel, as well as including a more faithful IHC model.

6. REFERENCES

1   K. A. Boahen, "Communicating neuronal ensembles between neuromorphic chips," in *Neuromorphic Systems Engineering*, T. S. Lande, Ed. Boston, MA: Kluwer Academic Publishers, 1998, pp. 229-259.

2   K. A. Boahen, "Point-to-point connectivity between neuromorphic chips using address events," *IEEE Transactions on Circuits and Systems II*, vol. 47, 2000, pp. 416-434.

3   E. Culurciello, R. Etienne-Cummings, and K. Boahen, "High dynamic range, arbitrated address event representation digital imager," *Proceedings IEEE International Symposium on Circuits and Systems*, 2001.

4   M. Barbaro, P.-Y. Burgi, A. Mortara, P. Nussbaum, and F. Heitger, "A 100×100 pixel silicon retina for gradient extraction with steering filter capabilities and temporal output coding," *IEEE Journal of Solid-State Circuits*, vol. 37, 2002, pp. 160-172.

5   K. A. Boahen, "A retinomorphic vision system," *IEEE Micro*, vol. 16, 1996, pp. 30-39.

6   C. M. Higgins and S. A. Shams, "A biologically inspired modular VLSI system for visual measurement of self-motion," *IEEE Sensors Journal*, vol. 2, 2002, pp. 508-528.

7   G. Indiveri, "Modeling selective attention using a neuromorphic analog VLSI device," *Neural Computation*, vol. 12, 2000, pp. 2857-2880.

8   G. Indiveri, A. M. Whatley, and J. Kramer, "A reconfigurable neuromorphic VLSI multi-chip system applied to visual motion computation," in *Proceedings of the Seventh Intl. Conference on Microelectronics for Neural, Fuzzy and Bio-inspired Systems; Microneuro'99*, Los Alamitos, CA, 1999.

9   S.-C. Liu, J. Kramer, G. Indiveri, T. Delbrück, T. Burg, and R. Douglas, "Orientation-selective aVLSI spiking neurons," in *Neural Networks: Special Issue on Spiking Neurons in Neuroscience and Technology*, Vol 14, No. 6/7, 2001, pp. 629-643.

10   T. Serrano-Gotarredona, A. G. Andreou, and B. Linares-Barranco, "AER image filtering architecture for vision-processing systems," *IEEE Transactions on Circuits and Systems I*, vol. 46, 1999, pp. 1064-1071.

11   S. R. Deiss, R. J. Douglas, and A. M. Whatley, "A pulse-coded communications infrastructure for neuromorphic systems," in *Pulsed Neural Networks*, W. a. B. Maass, C. M., Ed. Boston, MA: MIT Press, 1999, pp. 157-178.

12   D. H. Goldberg, G. Cauwenberghs, and A. Andreou, "Analog VLSI spiking neural network with address domain probabilistic synapses," in *Proceedings of the 2001 IEEE International Symposium on Circuits and Systems*, 2001.

13   S.-C. Liu and R. Douglas, "Temporal coding in a network of silicon integrate-and-fire neurons," *IEEE Transactions on Neural Network*, vol. 15, no.5, 2004, pp. 1305-1314.

14   A. van Schaik, "Building blocks for electronic spiking neural networks," *Neural Networks*, Vol. 14(6-7) , 2001, pp. 617-628.

15   P. Venier, A. Mortara, X. Arreguit, and E. A. Vittoz, "An integrated cortical layer for orientation enhancement," *IEEE Journal of Solid-State Circuits*, vol. 32, 1997, pp. 177-185.

16   J.P. Lazzaro and J. Wawrzynek, "A multi-sender asynchronous extension to the address-event protocol," *proceedings 16th Conference on Advanced Research in VLSI*, 1995, pp. 158-169.

17   N. Kumar, W. Himmelbauer, G. Cauwenberghs, & A. G. Andreou, "An Analog VLSI Chip with Asynchronous Interface for Auditory Feature Extraction," *IEEE Transactions On Circuits And Systems—II: Analog and Digital Signal Processing*, Vol. 45, No. 5, May 1998, pp. 600-606.

18   H. Abdalla, and T. Horiuchi, "An Ultrasonic Filterbank with Spiking Neurons", *IEEE ISCAS 2005*.

19   A. van Schaik and S-C. Liu, "AER EAR: A Matched Silicon Cochlea Pair with Address Event Representation Interface," *IEEE ISCAS 2005*.

20   A. van Schaik and S. Shamma, "A neuromorphic sound localizer for a smart MEMS system," *Analog Integrated Circuits & Signal Processing*, Vol. 39, 2004, pp 267-273.

21   A. van Schaik, E. Fragnière, and E. Vittoz, "Improved Silicon Cochlea using Compatible Lateral Bipolar Transistors," *Advances in Neural Information Processing Systems 8*, edited by D. Touretzky, et al., MIT press, Cambridge MA, 1996, pp. 671-677.

22   A. van Schaik, "An analog VLSI model of periodicity extraction in the human auditory system," *Analog Integrated Circuits & Signal Processing*, vol. 26, 2001, pp. 157-77.

23   A. van Schaik and R. Meddis, "Analog very large-scale integrated (VLSI) implementation of a model of amplitude-modulation sensitivity in the auditory brainstem," *Journal of the Acoustical Society of America*, vol. 105, 1999, pp. 811-821.

24   L. Watts, D. A. Kerns, R. F. Lyon, and C. A. Mead, "Improved implementation of the silicon cochlea," *IEEE Journal of Solid-State Circuits*, vol. 27, 1992, pp. 692-700.